Cubic Subdivision Schemes with Double Knots

Jiří Kosinka[a], Malcolm Sabin[b], Neil Dodgson[a]

[a]*Computer Laboratory, University of Cambridge, 15 JJ Thomson Avenue, Cambridge CB3 0FD, United Kingdom*
[b]*Numerical Geometry Ltd., 19 John Amner Close, Ely, Cambridge CB6 1DT, United Kingdom*

Abstract

We investigate univariate and bivariate binary subdivision schemes based on cubic B-splines with double knots. It turns out that double knots change the behaviour of a uniform cubic scheme from primal to dual. We focus on the analysis of new bivariate cubic schemes with double knots at extraordinary points. These cubic schemes produce C^1 surfaces with the original Doo-Sabin weights.

Keywords: Subdivision surface, binary subdivision, double knot, cubic B-splines, Doo-Sabin subdivision.

---

1. Introduction

Subdivision is a powerful and popular technique for generating free-form curves and surfaces with many applications in geometric modelling, multiresolution analysis, computer games, and the film industry. Since its introduction to computer graphics by Chaikin (1974) in the univariate case and Catmull and Clark (1978) and Doo and Sabin (1978) in the bivariate setting, it has been developed into a mature technology that is able to compete with other geometry representations, including NURBS.

Subdivision based on uniform B-splines is well understood (Warren and Weimer, 2001; Peters and Reif, 2008; Sabin, 2010). On the other hand, non-uniform bivariate schemes still pose challenges. In regular regions, one can rely on univariate results (Cohen et al., 1980; Schaefer and Goldman, 2009) and use tensor products. However, in extraordinary regions, the situation is more complex. One of the first to introduce bivariate non-uniform subdivision for arbitrary topology was Sederberg et al. (1998), but for degrees two and three only and with no continuity guarantees when multiple knots are present. Moreover, Qin and Wang (1999) showed that such non-uniform Doo-Sabin schemes diverge in some cases. A real breakthrough came only recently (Cashman et al., 2009b) and resulted in NURBS-compatible subdivision (Cashman et al., 2009a). Refer to the PhD dissertation of Cashman (2010) for more details.

Although the recent work on NURBS-compatible subdivision has answered many questions, the chase after a complete superset of subdivision surfaces and NURBS continues. In particular, in extraordinary regions, Cashman's framework does not handle either multiple knots or even-degree schemes, and it is far from obvious how it might be extended to cover these. Müller et al. (2006) did introduce a variant of Catmull-Clark which allows for varying knot intervals and direct evaluation of the limit surface. This work was later extended by Müller et al. (2010). However, since these schemes recreate Catmull-Clark patches in neighbourhoods of extraordinary vertices, double knots are not allowed to influence such regions.

These shortcomings motivated the research presented in this paper, which is to consider the behaviour of the simplest multiple knot, the double knot, in cubic schemes.

We use uniform cubic B-splines as our starting point. The corresponding subdivision scheme is categorised as *primal*, since every old vertex is mapped onto a new vertex in a subdivision step. On the other hand, it is known that Chaikin's scheme produces quadratic B-splines (Riesenfeld, 1975), which is an example of a *dual* scheme, i.e., a scheme that maps old edges onto new edges. These two notions generalise naturally to bivariate schemes, this time considering images of old vertices and old faces.

Email addresses: `Jiri.Kosinka@cl.cam.ac.uk` (Jiří Kosinka), `malcolm@geometry.demon.co.uk` (Malcolm Sabin), `Neil.Dodgson@cl.cam.ac.uk` (Neil Dodgson)

All schemes considered will be stationary (unless stated otherwise) and, except for a few illustrative schemes, non-uniform in the sense that double knots will be present. A subdivision step will consist of inserting a single knot (Section 2) or a double knot (Section 3) into the middle of every non-zero interval (general knot insertion rules will not be considered). Since a subdivision step consists of computing new vertices via linear combinations of old ones, it can be described using a *subdivision matrix*.

Our analyses of schemes with double knots are based on the approach introduced in Doo and Sabin (1978), i.e., using eigenanalysis of subdivision matrices and, in the bivariate case, Fourier partitioning. This will guarantee that our schemes with double knots possess the appropriate spectrum (Peters and Reif, 2008). Moreover, in order to show C^1 smoothness, we analyse the so called *natural configuration* of a scheme (Ball and Storry, 1988). This configuration is given by the eigenvector corresponding to the subdominant eigenvalue of a subdivision matrix. In turn, this configuration gives rise to the *characteristic map* of a scheme, which is the limit surface obtained by applying a scheme to its natural configuration. If this map and the spectrum satisfy certain properties, the original subdivision scheme produces C^1 surfaces (Peters and Reif, 1998).

Among other results, we show that the behaviour of a cubic uniform scheme locally changes from primal to dual with the insertion of double knots. This applies both to univariate and bivariate scenarios. Based on this observation, we design a bicubic scheme with all knots double, which is an odd-degree dual scheme. Due to its structure, no major modification of the existing framework is needed. We also discuss the relation of this new scheme to degree raising (Farin, 2002) and the possibility of adding even-degree schemes into Cashman's NURBS-compatible subdivision framework.

2. Single knot insertion

Consider subdivision schemes where we insert a single knot at the midpoint of every non-zero interval. We start by looking at the univariate case, then move on to tensor product schemes and finally analyse more general situations, namely configurations with n-fold symmetry, i.e., schemes with extraordinary faces of valency n.

2.1. Univariate schemes

For comparison, we briefly recall uniform cubic B-splines (Fig. 1). Note that the *support width* of the cubic B-spline basis function, i.e., the size of its region of influence, is 4. The subdivision matrix of the associated (uniform, stationary) primal binary scheme is

$$\frac{1}{8}\begin{pmatrix} \ddots & & & & & & \\ & 1 & 6 & \mathbf{1} & & & \\ & & 4 & \mathbf{4} & & & \\ & & 1 & \mathbf{6} & 1 & & \\ & & & \mathbf{4} & 4 & & \\ & & & \mathbf{1} & 6 & 1 & \\ & & & & & & \ddots \end{pmatrix}. \tag{1}$$

The column in bold, $(\mathbf{1},\mathbf{4},\mathbf{6},\mathbf{4},\mathbf{1})/8$, represents the *mask* of this scheme. The rows of the matrix are *stencils* (in this case there are two of them) and each row sums to one. We call this uniform scheme, which produces C^2 curves, the $\mathcal{U}$ scheme. For a detailed treatment of univariate subdivision schemes (including end conditions) refer to Sabin (2010).

We now consider the situation where one of the knots is doubled. The corresponding cubic basis functions are shown in Fig. 2. Note that the basis functions influenced by the double knot have support width 3 only.

Using a standard knot insertion algorithm (Cohen et al., 1980; Boehm, 1980) we insert a knot into the middle of every non-zero knot interval: the double knot thus remains the only double knot. Repeating this process simply reproduces the whole situation, but scaled down by the factor of 2. This yields a stationary scheme.

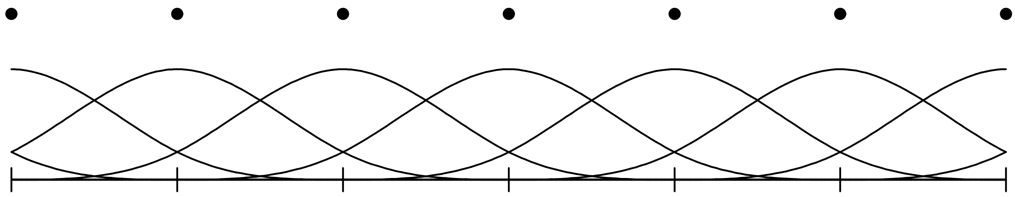

Figure 1: Cubic B-spline basis function(s). The black points correspond to the natural configuration of the scheme.

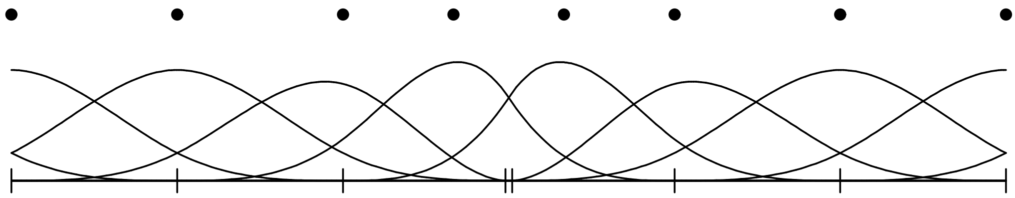

Figure 2: Cubic basis functions close to a double knot. The black points correspond to the natural configuration of the scheme.

Using knot insertion, one can derive that the subdivision matrix of this scheme is

$$\frac{1}{16}\begin{pmatrix} \ddots & & & & & & & \\ & 2 & & & & & & \\ & 8 & & & & & & \\ & 12 & 2 & & & & & \\ & 8 & 8 & & & & & \\ & 2 & \mathbf{11} & \mathbf{3} & & & & \\ & & \mathbf{4} & \mathbf{12} & & & & \\ & & & \mathbf{12} & \mathbf{4} & & & \\ & & & \mathbf{4} & \mathbf{12} & & & \\ & & & & \mathbf{12} & \mathbf{4} & & \\ & & & & \mathbf{3} & \mathbf{11} & 2 & \\ & & & & & 8 & 8 & \\ & & & & & 2 & 12 & \\ & & & & & & 8 & \\ & & & & & & 2 & \\ & & & & & & & \ddots \end{pmatrix}. \tag{2}$$

The part of the matrix which differs from the standard matrix (1), i.e., the part which is affected by the double knot, is emphasized in bold. Note that the stencils (rows) still sum to 1. However, unlike the uniform scheme, which has a single mask, this modified scheme, which we will call the $\mathcal{M}$ scheme, is now given by 5 different masks (columns).

Taking a closer look at the matrix, we see that away from the double knot, one obtains the standard primal binary subdivision scheme based on uniform cubic B-splines (cf. Section 2.1). On the other hand, locally in the vicinity of the double knot, it resembles a dual scheme. Examples and comparison of the schemes mentioned above are shown in Fig. 3.

For future use, we remark that, in the case of the $\mathcal{U}$ scheme, the neighbourhood of each point corresponding to a knot is influenced by 5 original control points. In contrast, the same influence in the $\mathcal{M}$ scheme is 6 control points, 3 on each side, for the point corresponding to the double knot. On the other hand, first and second order behaviour of both the schemes is the same.

Since the $\mathcal{M}$ scheme is based on B-splines, we know that the continuity of the limit curve is only C^1 at the point corresponding to the double knot. However, for illustrative purposes, we also follow the analysis used in Sabin (2010),

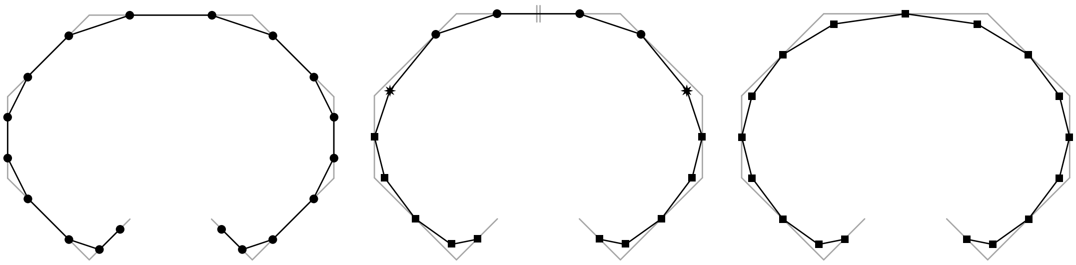

a) Quadratic - uniform b) Cubic with one double knot c) Cubic - uniform

Figure 3: Original polygon (grey) and the polygon after one subdivision step (black). Markers bullet, square, and star denote points computed using quadratic, cubic, and 'transitional' stencils, respectively.

Section 15.1.

The matrix that needs to be analysed here is the central block of (2), i.e., the part of (2) that is influenced by the double knot

$$\frac{1}{16}\begin{pmatrix} \mathbf{2} & 11 & 3 & & & \\ & \mathbf{4} & 12 & & & \\ & & \mathbf{12} & \mathbf{4} & & \\ & & \mathbf{4} & \mathbf{12} & & \\ & & & 12 & \mathbf{4} & \\ & & & 3 & 11 & \mathbf{2} \end{pmatrix}. \tag{3}$$

Exploiting its block diagonal structure (in bold), we find that its spectrum is $\left\{1, \frac{1}{2}, \frac{1}{4}, \frac{1}{4}, \frac{1}{8}, \frac{1}{8}\right\}$ and the corresponding unnormalised eigencolumns (right eigenvectors) and eigenrows (left eigenvectors) are

$$\begin{array}{cccccc} 1 & 1/2 & 1/4 & 1/4 & 1/8 & 1/8 \\ \begin{pmatrix} \vdots \\ 1 \\ 1 \\ 1 \\ 1 \\ 1 \\ 1 \\ 1 \\ 1 \\ \vdots \end{pmatrix} & \begin{pmatrix} \vdots \\ -9 \\ -6 \\ -3 \\ -1 \\ 1 \\ 3 \\ 6 \\ 9 \\ \vdots \end{pmatrix} & \begin{pmatrix} \vdots \\ 26 \\ 11 \\ 2 \\ 0 \\ 0 \\ 2 \\ 11 \\ 26 \\ \vdots \end{pmatrix} & \begin{pmatrix} \vdots \\ -26 \\ -11 \\ -2 \\ 0 \\ 0 \\ 2 \\ 11 \\ 26 \\ \vdots \end{pmatrix} & \begin{pmatrix} \vdots \\ 4 \\ 1 \\ 0 \\ 0 \\ 0 \\ 0 \\ 1 \\ 4 \\ \vdots \end{pmatrix} & \begin{pmatrix} \vdots \\ -4 \\ -1 \\ 0 \\ 0 \\ 0 \\ 0 \\ 1 \\ 4 \\ \vdots \end{pmatrix} \end{array} \qquad \begin{array}{cc} 1 & (0,0,1,1,0,0) \\ 1/2 & (0,0,-1,1,0,0) \\ 1/4 & (0,1,-1,-1,1,0) \\ 1/4 & (0,1,-3,3,-1,0) \\ 1/8 & (2,-11,9,9,-11,2) \\ 1/8 & (-2,11,-21,21,-11,2). \end{array} \tag{4}$$

The first eigenrow gives the *limit stencil* of the scheme, i.e., the stencil for computing the limit point of the scheme corresponding to the double knot. The second eigenrow, associated with the subdominant eigenvalue $1/2$, gives the (unscaled) limit first derivative when applied to the data.

The subdominant eigencolumn gives the natural configuration of the scheme, see Fig. 2. Denoting the first four eigencolumns C_0, C_1, C_2, and C_3, one can check that, in contrast to the uniform case, they do not satisfy the relation $C_2 = \alpha C_0 + \beta C_1^2$ for any real parameters α and β. However, using limit stencils or the basis functions of the $\mathcal{M}$ scheme one can verify that C_0, C_1, and C_2 generate monomials of degree zero, one, and two, respectively (Warren, 1995). In other words, the scheme can generate an arbitrary quadratic polynomial. On the other hand, since C_3 generates $x^2\mathrm{sgn}(x)$, the second derivative is generically not continuous at the point corresponding to the double knot and thus the scheme is C^1 only.

2.2. Tensor product schemes

Consider the tensor products of the above univariate schemes, the uniform one, $\mathcal{U}$, and the modified one, $\mathcal{M}$. These two schemes give three different tensor product scenarios. The one given by $\mathcal{U} \times \mathcal{U}$ yields the well known bicubic

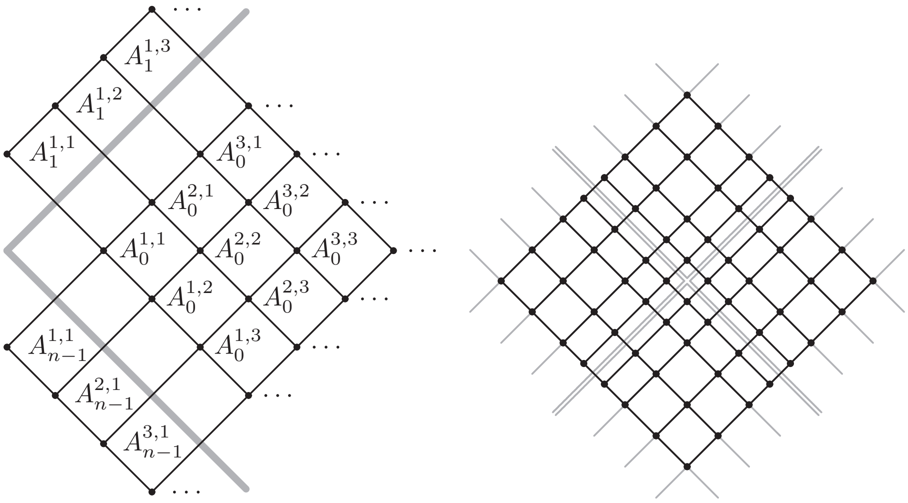

Figure 4: Left: Labelling of vertices (for any dual scheme with single or double knots). The lower index represents the segment (quadrant when $n = 4$) a vertex lies in. Right: The natural configuration of the $\mathcal{M} \times \mathcal{M}$ scheme.

uniform subdivision scheme. A generalisation of this scenario to arbitrary valencies leads to a family of schemes, the first of which was introduced by Catmull and Clark (1978).

The two remaining tensor product schemes behave as the bicubic one away from irregular regions, so we will focus only on their local behaviour under the influence of double knots.

The tensor product $\mathcal{U} \times \mathcal{M}$ yields a scheme with a double knot along a line on the surface. In the vicinity of the double knot we obtain the behaviour governed by 'cubic times quadratic', cf. Section 2.1. From the tensor product structure we can immediately conclude that the scheme is only C^1 at the line corresponding to the double knot.

A similar argument applies to the $\mathcal{M} \times \mathcal{M}$ scheme. However, since this scenario can be easily generalised to arbitrary valencies (just as $\mathcal{U} \times \mathcal{U}$), we devote the following section to it. This is a first step in our attempt to generalise Cashman's framework to multiple knots at extraordinary vertices.

2.2.1. The $\mathcal{M} \times \mathcal{M}$ scheme

Taking the tensor product $\mathcal{M} \times \mathcal{M}$ gives a scheme with two lines of double knots meeting at the central face of the control mesh (not a vertex as in the single-knot case). This gives the bivariate behaviour at a face of valency 4 where two double-knot lines cross. It is locally governed by dual 'quadratic times quadratic' B-splines, yet it is not the same as the tensor product biquadratic scheme, since the limit functions are piecewise cubic, not quadratic.

Now we introduce notation which will apply also to the general case $n \geq 3$. Let capital letters $A_k^{1,1}, A_k^{1,2}, \ldots$ denote original vertices and small letters $a_k^{1,1}, a_k^{1,2}, \ldots$ new ones, after one subdivision step (we insert a knot in the middle of every non-zero interval), where $k \in \{0, \ldots, n-1\}$ denotes the *segment* (quadrant when $n = 4$) of the respective vertices, see Fig. 4. Such lower indices will be treated modulo n. Using the (inverse) discrete Fourier transform, we set

$$A_k^{i,j} = \sum_{\omega=0}^{n-1} \tilde{A}_\omega^{i,j} e^{\frac{2\pi \mathbf{i}}{n}\omega k} \quad \text{and} \quad a_k^{i,j} = \sum_{\omega=0}^{n-1} \tilde{a}_\omega^{i,j} e^{\frac{2\pi \mathbf{i}}{n}\omega k}, \tag{5}$$

where $\mathbf{i} = \sqrt{-1}$ is the complex unit and ω is the Fourier index. In this section we focus on the case when $n = 4$. We look at more general values of n in Section 2.3. This analysis follows that pioneered by Doo and Sabin (1978).

We use the labelling of vertices shown in Fig. 4 and stencils derived by taking the tensor product of (2) with itself. Let $u = e^{-\frac{2\pi \mathbf{i}}{n}\omega}$, $\bar{u} = e^{\frac{2\pi \mathbf{i}}{n}\omega}$ and $\lambda_\omega = \frac{18+6(u+\bar{u})+u^2+\bar{u}^2}{32}$. Then in the Fourier domain

$$
256\left(\begin{array}{c}
\tilde{a}_\omega^{1,1} \\ \hline
\tilde{a}_\omega^{1,2} \\
\tilde{a}_\omega^{2,1} \\ \hline
\tilde{a}_\omega^{2,2} \\ \hline\hline
\tilde{a}_\omega^{1,3} \\
\tilde{a}_\omega^{3,1} \\ \hline
\tilde{a}_\omega^{2,3} \\ \hline
\tilde{a}_\omega^{3,2} \\ \hline
\tilde{a}_\omega^{3,3}
\end{array}\right)
=
\left(\begin{array}{c|cc|c||cc|c|c|c}
\mathbf{256\boldsymbol{\lambda_\omega}} & & & & & & & & \\ \hline
48(3+u) & \mathbf{48} & \mathbf{16u} & & & & & & \\
48(3+\bar{u}) & \mathbf{16\bar{u}} & \mathbf{48} & & & & & & \\ \hline
144 & 48 & 48 & \mathbf{16} & & & & & \\ \hline\hline
12(3+u) & 132 & 44u & 0 & \mathbf{24} & \mathbf{8u} & & & \\
12(3+\bar{u}) & 44\bar{u} & 132 & 0 & \mathbf{8\bar{u}} & \mathbf{24} & & & \\ \hline
36 & 132 & 12 & 44 & 24 & 0 & \mathbf{8} & & \\ \hline
36 & 12 & 132 & 44 & 0 & 24 & 0 & \mathbf{8} & \\ \hline
9 & 33 & 33 & 121 & 6 & 6 & 22 & 22 & \mathbf{4}
\end{array}\right)
\cdot
\left(\begin{array}{c}
\tilde{A}_\omega^{1,1} \\ \hline
\tilde{A}_\omega^{1,2} \\
\tilde{A}_\omega^{2,1} \\ \hline
\tilde{A}_\omega^{2,2} \\ \hline\hline
\tilde{A}_\omega^{1,3} \\
\tilde{A}_\omega^{3,1} \\ \hline
\tilde{A}_\omega^{2,3} \\ \hline
\tilde{A}_\omega^{3,2} \\ \hline
\tilde{A}_\omega^{3,3}
\end{array}\right). \tag{6}
$$

Note that we include a grid of 3×3 points in each segment. This corresponds to the fact that 3 points on each side influence the neighbourhood of the point corresponding to the double knot in the $\mathcal{M}$ scheme (cf. Section 2.1).

The matrix has a lower block diagonal structure (with diagonal blocks in bold) and thus finding its spectrum is essentially trivial — one block at a time. This was achieved by carefully sorting the vertices in their columns. We get the following eigenvalues of (6)

$$
\left\{\lambda_\omega, \frac{1}{4}, \frac{1}{8}, \frac{1}{8}, \frac{1}{16}, \frac{1}{16}, \frac{1}{32}, \frac{1}{32}, \frac{1}{64}\right\}. \tag{7}
$$

Except for the first eigenvalue λ_ω, all values in the above set are n-fold eigenvalues. For $n = 4$,

$$
16\lambda_\omega = 9 + 6\cos\left(\frac{\pi\omega}{2}\right) + \cos(\pi\omega). \tag{8}
$$

Looking at different Fourier indices gives the dominant eigenvalues

$$
\begin{array}{c||c|c|c|c}
\omega & 0 & 1 & 2 & 3 \\ \hline
\lambda_\omega & 1 & \frac{1}{2} & \frac{1}{4} & \frac{1}{2}
\end{array}. \tag{9}
$$

Thus the complete spectrum of the original subdivision matrix for $n = 4$ (36×36) reads

$$
\left\{1, \frac{1}{2}, \frac{1}{2}, \underbrace{\frac{1}{4}}_{5\times}, \underbrace{\frac{1}{8}}_{8\times}, \underbrace{\frac{1}{16}}_{8\times}, \underbrace{\frac{1}{32}}_{8\times}, \underbrace{\frac{1}{64}}_{4\times}\right\}. \tag{10}
$$

The eigendecomposition of the matrix (6) yields the obligatory column vector

$$
(1, 1, 1, 1, 1, 1, 1, 1, 1)^\top \tag{11}
$$

associated with $\lambda_0 = 1$. We also obtain the column vector

$$
(2, 4 - 2\mathbf{i}, 4 + 2\mathbf{i}, 6, 7 - 5\mathbf{i}, 7 + 5\mathbf{i}, 9 - 3\mathbf{i}, 9 + 3\mathbf{i}, 12)^\top \tag{12}
$$

and its complex conjugate associated with $\lambda_1 = 1/2$ and $\lambda_3 = 1/2$. The real and imaginary parts of (12) give the natural configuration of the $\mathcal{M} \times \mathcal{M}$ scheme depicted in Fig. 4, right.

As was to be expected, we obtained a scheme that locally resembles the biquadratic B-spline subdivision scheme. In fact, the left upper block (4×4, delimited by $||$) of the matrix (6) is exactly the same as in the single-knot biquadratic case. Now the question is how to generalise the stencil for the new points $a_k^{1,1}$ to accommodate irregular valencies as well. We answer this question, along with the question of C^1 continuity, in the following section.

2.3. Arbitrary valency with n-fold symmetry

Let us assume that n double knots meet at a point corresponding to a face with valency n in the control net. By n-fold symmetry we mean that all these knots are double knots. All the other knots are single. This scheme will be denoted $\mathcal{M}_n$.

Standard eigenanalysis, including the Fourier partitioning we used on the $\mathcal{M} \times \mathcal{M}$ scheme, can be employed to investigate this situation as well. The labelling of vertices we use is consistent with the one in the regular setting, see Fig. 4. The lower index, k, now ranges from 0 to $n-1$, considered modulo n.

The important fact to observe is that except for the vertices $a_k^{1,1}$, all the other new vertices, i.e., $a_k^{i,j}$ with $i+j>2$, depend solely on the old vertices from their segment (with index k) and up to two of their neighbouring segments (with indices $k-1$ and $k+1$). Therefore, the matrix (6) remains the same for every n except for its first element λ_ω. More precisely, the only change occurs for $a_k^{1,1}$,

$$a_k^{1,1} = \sum_{l=0}^{n-1} \alpha_l A_{l+k}^{1,1}, \tag{13}$$

where α_l are the weights for computing the new vertices $a_k^{1,1}$ from the old ones $A_k^{1,1}$. In the Fourier domain (see (5)) this becomes

$$\tilde{a}_\omega^{1,1} = \tilde{A}_\omega^{1,1} \sum_{l=0}^{n-1} \alpha_l e^{\frac{2\pi \mathbf{i}}{n}\omega l}. \tag{14}$$

Consequently, the eigenvalues λ_ω for general valency n are

$$\lambda_\omega = \sum_{l=0}^{n-1} \alpha_l e^{\frac{2\pi \mathbf{i}}{n}\omega l}. \tag{15}$$

It only remains to choose the weights α_l. Observe that equation (15) is of the same type as (5), i.e., the sequence of eigenvalues λ_ω for $\omega = 0 \dots n-1$ is the inverse discrete Fourier transform of the weights α_l with $l = 0 \dots n-1$. Therefore, we can prescribe any (reasonable) set of eigenvalues and compute the weights α_l associated with them using the discrete Fourier transform. However, in order to obtain a C^1 scheme with bounded curvature (Warren and Weimer (2001); Peters and Reif (2008)), the eigenvalues must follow the pattern given by

$$\begin{array}{c||c|c|c|c|c|c} \omega & 0 & 1 & 2 & \dots & n-2 & n-1 \\ \hline \lambda_\omega & 1 & \lambda_1 < 1 & \lambda_1^2 & \lambda_\omega < \lambda_1^2 & \lambda_1^2 & \lambda_1 \end{array}. \tag{16}$$

There are several variants that yield a well-behaved scheme; see Section 6.2 of Peters and Reif (2008) for more details. In this paper, we use the original Doo-Sabin weights (Doo and Sabin, 1978)

$$\alpha_l = \frac{\delta_{l,0}}{4} + \frac{3 + 2\cos(\frac{2\pi l}{n})}{4n} \tag{17}$$

that generalise the biquadratic case to any valency. Looking at different Fourier indices gives (cf. (9))

$$\begin{array}{c||c|c|c|c|c|c} \omega & 0 & 1 & 2 & \dots & n-2 & n-1 \\ \hline \lambda_\omega & 1 & \frac{1}{2} & \frac{1}{4} & \dots & \frac{1}{4} & \frac{1}{2} \end{array}, \tag{18}$$

where all the 'middle' eigenvalues are equal to $\frac{1}{4}$. One can check that this choice agrees with λ_ω when $n=4$, i.e., in the case of the $\mathcal{M} \times \mathcal{M}$ scheme; cf. (9).

Combining these eigenvalues with the remaining ones, we obtain the whole spectrum of the original subdivision matrix ($9n \times 9n$)

$$\left\{ 1, \frac{1}{2}, \frac{1}{2}, \underbrace{\frac{1}{4}}_{2n-3\times}, \underbrace{\frac{1}{8}}_{2n\times}, \underbrace{\frac{1}{16}}_{2n\times}, \underbrace{\frac{1}{32}}_{2n\times}, \underbrace{\frac{1}{64}}_{n\times} \right\}. \tag{19}$$

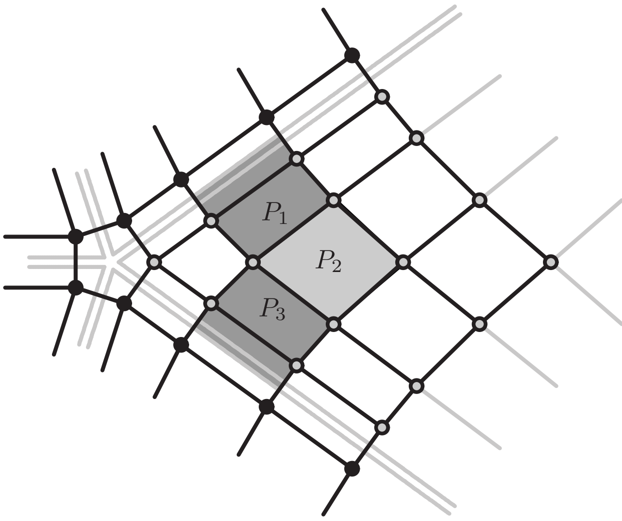

Figure 5: Three bicubic patches of one segment of the characteristic map of $\mathcal{M}_n$. The patch P_2 is given in terms of the control points shown in grey.

As for the $\mathcal{M} \times \mathcal{M}$ scheme, we see that $\mathcal{M}_n$ resembles the Doo-Sabin scheme in the vicinity of an extraordinary face. It thus comes as no surprise that $\mathcal{M}_n$ produces C^1 surfaces. We prove this fact by using Corollary 4.1 from Peters and Reif (1998); see Peters and Reif (2008) for a complete treatment of continuity of subdivision surfaces.

We remark that we need to include 4×4 vertices in each segment to prove C^1 continuity; see Fig. 5. As for $\mathcal{M} \times \mathcal{M}$, the column vector associated with $\lambda_0 = 1$ is a column of 1s. With $c = \cos \frac{2\pi}{n}$, $s = \sin \frac{2\pi}{n}$, and defining $g = 6(1304c + 3255)$ we obtain the column vector (displayed as a matrix following our labelling of vertices, the element corresponding to $A_0^{1,1}$ lies in the left bottom corner)

$$\frac{1}{g}\begin{pmatrix} 2170(4c+5) & 186(39c+70) & 15(459c+1085) & g \\ 1085(5c+7) & 93(47c+105) & 6(841c+2170) & 15(459c+1085) \\ 2170(c+2) & 930(2c+7) & 93(47c+105) & 186(39c+70) \\ 2170 & 2170(c+2) & 1085(5c+7) & 2170(4c+5) \end{pmatrix} + \frac{1085\mathbf{i}s}{g}\begin{pmatrix} 8 & 6 & 3 & 0 \\ 5 & 3 & 0 & -3 \\ 2 & 0 & -3 & -6 \\ 0 & -2 & -5 & -8 \end{pmatrix} \tag{20}$$

and its complex conjugate associated with $\lambda_1 = 1/2$ and $\lambda_{n-1} = 1/2$. These give the normalised natural configuration (Peters and Reif, 1998) of the scheme; see Fig. 6.

Since $\mathcal{M}_n$ is based on bicubic B-splines, each segment of its characteristic map $\Psi(u, v)$ consists of three bicubic patches P_i, $i = 1, 2, 3$; see Fig. 5. Moreover, since we employ symmetric weights, $\mathcal{M}_n$ is a symmetric subdivision scheme and thus it is sufficient to inspect only one segment of its characteristic map. We express the three patches of the segment $\Psi_0(u, v)$ of the map with index $k = 0$ in Bernstein-Bézier form. According to the above mentioned corollary, we need to show that $\frac{\partial P_i}{\partial v}$ lies in the first quadrant of $\mathbb{C}$, the complex plane.

For the first patch, P_1, the Bernstein-Bézier form of its derivative $\frac{\partial P_1}{\partial v}$ (up to a positive multiple) reads

$$\begin{pmatrix} 558(34c+35) & 558(33c+35) & 558(31c+35) & 90(170c+217) \\ 186(101c+105) & 186(97c+105) & 186(89c+105) & 6(2329c+3255) \\ 31(473c+525) & 31(421c+525) & 31(317c+525) & 25(277c+651) \end{pmatrix} + 3255\mathbf{i}s\begin{pmatrix} 6 & 6 & 6 & 6 \\ 6 & 6 & 6 & 6 \\ 5 & 5 & 5 & 5 \end{pmatrix}. \tag{21}$$

Indeed, since $-1/2 \leq c < 1$ and $s > 0$, all the control points lie in the first quadrant of $\mathbb{C}$ for all values of $n \geq 3$. The same holds for the remaining two patches P_2 and P_3 of $\Psi_0(u, v)$. Their derivatives $\frac{\partial P_2}{\partial v}$ and $\frac{\partial P_3}{\partial v}$ (up to a positive

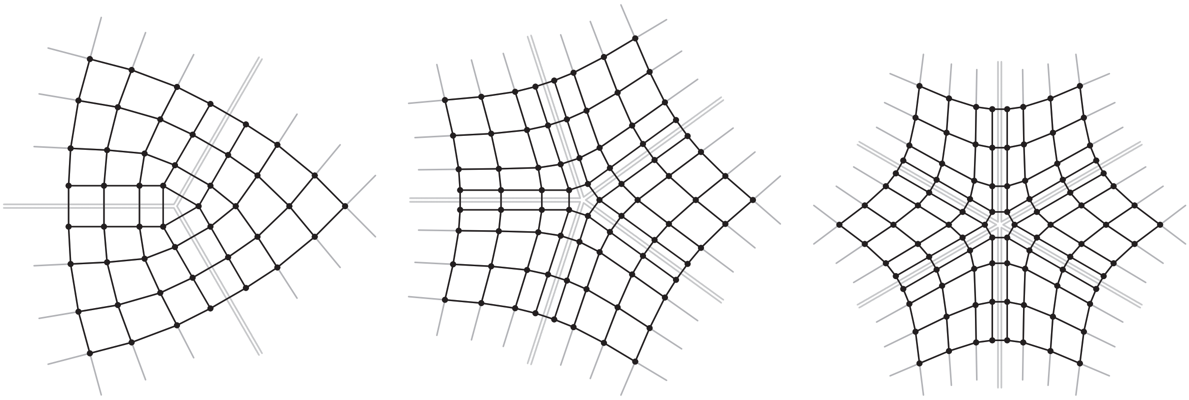

Figure 6: The natural configurations of $\mathcal{M}_n$ for n equal to 3, 5 and 6.

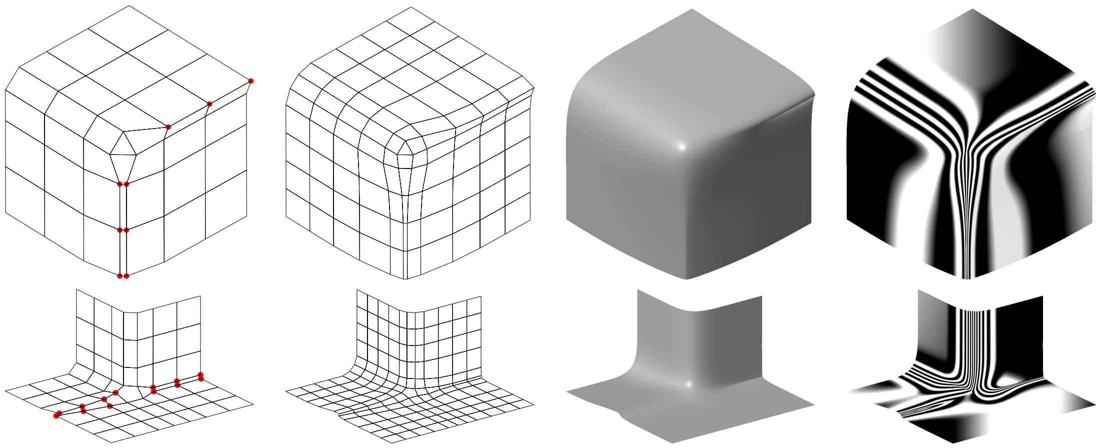

Figure 7: Top: An example of $\mathcal{M}_3$. Bottom: An example of $\mathcal{M}_5$. From left to right: The control mesh, the mesh after one refinement step, the limit surface, and reflection lines on the limit surface. Control vertices that have been moved with respect to their positions created by knot insertion are marked by red bullets.

multiple) are given by

$$\begin{pmatrix} 90(170c+217) & 18(739c+1085) & 18(579c+1085) & 90(89c+217) \\ 6(2329c+3255) & 18(633c+1085) & 18(429c+1085) & 18(269c+1085) \\ 25(277c+651) & 3(1341c+5425) & 3(481c+5425) & 15(-37c+1085) \end{pmatrix} + 3255\mathbf{i}s \begin{pmatrix} 6 & 6 & 6 & 6 \\ 6 & 6 & 6 & 6 \\ 5 & 5 & 5 & 5 \end{pmatrix} \tag{22}$$

and

$$\begin{pmatrix} 25(277c+651) & 3(1341c+5425) & 3(481c+5425) & 15(-37c+1085) \\ 124(-c+105) & 372(-9c+35) & 372(-13c+35) & 372(-16c+35) \\ 31(-317c+525) & 93(-123c+175) & 93(-131c+175) & 93(-137c+175) \end{pmatrix} + 3255\mathbf{i}s \begin{pmatrix} 5 & 5 & 5 & 5 \\ 4 & 4 & 4 & 4 \\ 5 & 5 & 5 & 5 \end{pmatrix}. \tag{23}$$

This concludes the proof of C^1 continuity of the $\mathcal{M}_n$ scheme at (extraordinary) faces where n double knots meet.

Even though the knot configuration is linked with the mesh structure, a control mesh for $\mathcal{M}_n$ can be automatically generated from a Catmull-Clark control mesh (i.e., a $\mathcal{U}_n$ mesh) by standard B-spline knot insertion. The user thus obtains extra degrees of freedom without losing C^1 smoothness. Examples of $\mathcal{M}_3$ and $\mathcal{M}_5$ are shown in Fig. 7.

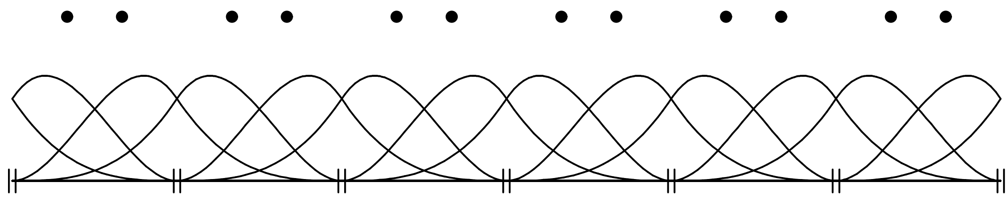

Figure 8: Cubic basis functions where all knots are double. The black points correspond to the natural configuration of the $\mathcal{D}$ scheme.

The control meshes were created automatically from simple Catmull-Clark control meshes and only some of the new vertices have been moved.

3. Double knot insertion

Now consider the case when every knot is doubled and a subdivision step inserts a double knot into the middle of every non-zero knot interval. We start with a univariate scheme and then move on to its bivariate generalisation.

3.1. A univariate scheme

In this scenario where all initial knots are double (see Fig. 8), it would be possible to explore the insertion of single knots, but this would rapidly simplify to multiple disjoint instances of the previous case $\mathcal{M}$. We therefore explore the more interesting case where the inserted knots are also double, thus retaining the all-knots-double structure. This gives a stationary scheme we denote $\mathcal{D}$. Moreover, as discussed in Section 4, it is closely related to degree-raising.

One can show that the corresponding subdivision matrix that needs to be analysed reads

$$\frac{1}{8}\begin{pmatrix} \mathbf{1} & 5 & 2 & & & \\ & \mathbf{2} & 5 & 1 & & \\ & & \mathbf{6} & \mathbf{2} & & \\ & & \mathbf{2} & \mathbf{6} & & \\ & & 1 & 5 & \mathbf{2} & \\ & & & 2 & 5 & \mathbf{1} \end{pmatrix}. \tag{24}$$

Again, exploiting its block diagonal structure (in bold), we find that its eigendecomposition is

$$\begin{array}{cccccc} 1 & 1/2 & 1/4 & 1/4 & 1/8 & 1/8 \\ \begin{pmatrix} \vdots \\ 1 \\ 1 \\ 1 \\ 1 \\ 1 \\ 1 \\ 1 \\ 1 \\ \vdots \end{pmatrix} & \begin{pmatrix} \vdots \\ -5 \\ -4 \\ -2 \\ -1 \\ 1 \\ 2 \\ 4 \\ 5 \\ \vdots \end{pmatrix} & \begin{pmatrix} \vdots \\ 8 \\ 5 \\ 1 \\ 0 \\ 0 \\ 1 \\ 5 \\ 8 \\ \vdots \end{pmatrix} & \begin{pmatrix} \vdots \\ -8 \\ -5 \\ -1 \\ 0 \\ 0 \\ 1 \\ 5 \\ 8 \\ \vdots \end{pmatrix} & \begin{pmatrix} \vdots \\ 2 \\ 1 \\ 0 \\ 0 \\ 0 \\ 0 \\ 1 \\ 2 \\ \vdots \end{pmatrix} & \begin{pmatrix} \vdots \\ -2 \\ -1 \\ 0 \\ 0 \\ 0 \\ 0 \\ 1 \\ 2 \\ \vdots \end{pmatrix} \end{array} \qquad \begin{array}{cc} 1 & (0,0,1,1,0,0) \\ 1/2 & (0,0,-1,1,0,0) \\ 1/4 & (0,1,-1,-1,1,0) \\ 1/4 & (0,1,-2,2,-1,0) \\ 1/8 & (1,-5,4,4,-5,1) \\ 1/8 & (-1,5,-6,6,-5,1)\,. \end{array} \tag{25}$$

The subdominant eigencolumn gives the natural configuration of the scheme; see Fig. 8. Since this scheme is based on B-splines, we know that it produces C^1 curves. The above eigendecomposition confirms this.

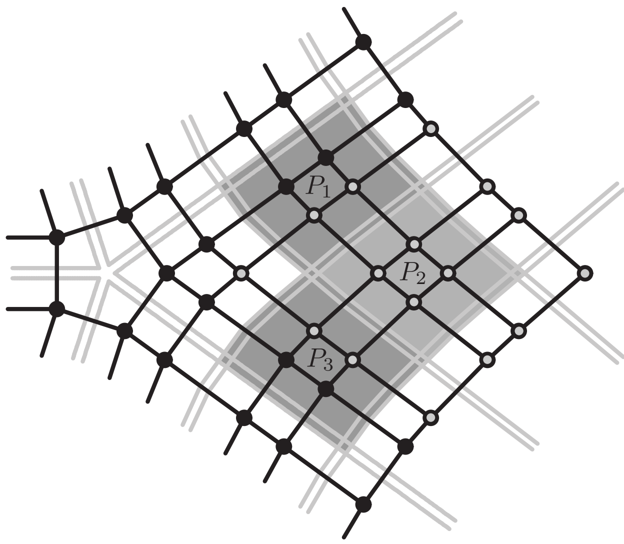

Figure 9: Three bicubic patches of one segment of the characteristic map of $\mathcal{D}_n$. The patch P_2 is given in terms of the control points shown in grey.

3.2. Tensor product: the $\mathcal{D} \times \mathcal{D}$ scheme

The analysis of the $\mathcal{D} \times \mathcal{D}$ scheme, and its generalisation to arbitrary valencies, shares a lot of features with the bivariate schemes based on $\mathcal{M}$. We use the same notation and labelling as in the previous section.

However, one of the most important differences from the Doo-Sabin and $\mathcal{M} \times \mathcal{M}$ schemes is that not only $a_k^{1,1}$, but also $a_k^{1,2}$, $a_k^{2,1}$ and $a_k^{2,2}$ depend on *all* the old $A^{1,1}$ points. From the stencils of the univariate scheme $\mathcal{D}$ it follows that

$$\begin{aligned}
64a_k^{1,1} &= 12A_{k-1}^{1,1} + 36A_k^{1,1} + 12A_{k+1}^{1,1} + 4A_{k+2}^{1,1}, \\
64a_k^{1,2} &= 10A_{k-1}^{1,1} + 30A_k^{1,1} + 6A_{k+1}^{1,1} + 2A_{k+2}^{1,1} + 12A_k^{1,2} + 4A_{k-1}^{2,1}, \\
64a_k^{2,1} &= 6A_{k-1}^{1,1} + 30A_k^{1,1} + 10A_{k+1}^{1,1} + 2A_{k+2}^{1,1} + 4A_{k+1}^{1,2} + 12A_k^{2,1}, \\
64a_k^{2,2} &= 5A_{k-1}^{1,1} + 25A_k^{1,1} + 5A_{k+1}^{1,1} + A_{k+2}^{1,1} + 10A_k^{2,1} + 2A_{k+1}^{2,1} + 10A_k^{1,2} + 2A_{k-1}^{1,2} + 4A_k^{2,2}.
\end{aligned} \tag{26}$$

Now we observe that the new $a_k^{1,2}$, $a_k^{2,1}$ and $a_k^{2,2}$ can be expressed in terms of $a_k^{1,1}$ and old vertices from segments with index k and the two neighbouring segments with indices $k-1$ and $k+1$ only:

$$\begin{aligned}
64a_k^{1,2} &= 32a_k^{1,1} + 4A_{k-1}^{1,1} + 12A_k^{1,1} + 12B_k^{1,2} + 4A_{k-1}^{2,1}, \\
64a_k^{2,1} &= 32a_k^{1,1} + 12A_k^{1,1} + 4A_{k+1}^{1,1} + 4A_{k+1}^{1,2} + 12A_k^{2,1}, \\
64a_k^{2,2} &= 16a_k^{1,1} + 2A_{k-1}^{1,1} + 16A_k^{1,1} + 2A_{k+1}^{1,1} + 10A_k^{1,2} + 2A_{k+1}^{1,2} + 10A_k^{2,1} + 2A_{k-1}^{2,1} + 4A_k^{2,2}.
\end{aligned} \tag{27}$$

Consequently, when passing from $n = 4$ to general valency, we only need to adjust the weights for $a_k^{1,1}$, the other new vertices then follow from (27) or are not affected at all (vertices $a_k^{i,j}$ with $i > 2$ or $j > 2$). Therefore, we do not discuss the case $n = 4$ separately.

3.3. Arbitrary valency with n-fold symmetry

We denote $\mathcal{D}_n$ the generalisation of the tensor product scheme $\mathcal{D} \times \mathcal{D}$ to valency n. Using the same approach as in Section 2.3 with the same labelling and order of vertices as in matrix (6), one can derive that the subdivision matrix

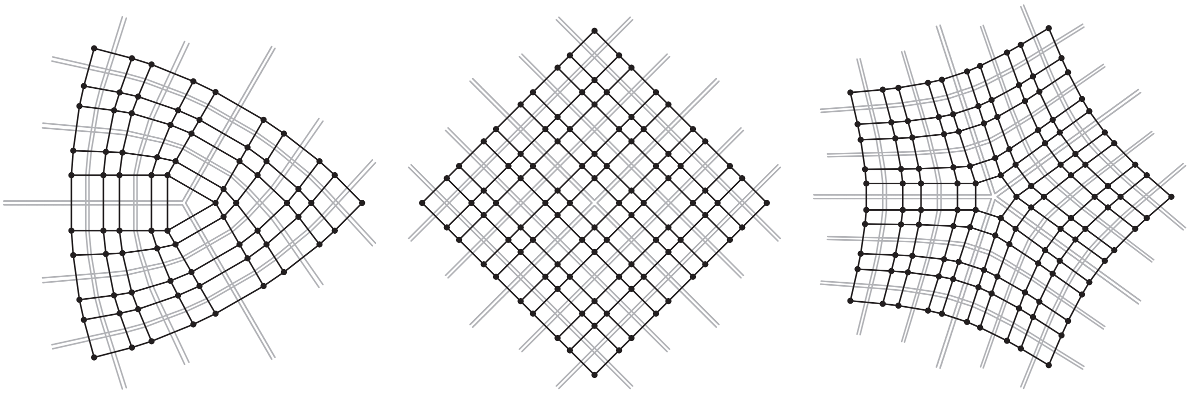

Figure 10: The natural configurations of $\mathcal{D}_n$ for n equal to 3, 4 and 5.

of $\mathcal{D}_n$ in the Fourier domain reads

$$\frac{1}{64}\left(\begin{array}{c|cc|c||cc|c|c|c}
\boldsymbol{64\lambda_\omega} & & & & & & & & \\ \hline
32\lambda_\omega+12+4u & \mathbf{12} & \mathbf{4u} & & & & & & \\
32\lambda_\omega+12+4\bar{u} & \mathbf{4\bar{u}} & \mathbf{12} & & & & & & \\ \hline
16\lambda_\omega+16+2(u+\bar{u}) & 10+2\bar{u} & 10+2u & \mathbf{4} & & & & & \\ \hline\hline
12+4u & 30 & 10u & 0 & \mathbf{6} & \mathbf{2u} & & & \\
12+4\bar{u} & 10\bar{u} & 30 & 0 & \mathbf{2\bar{u}} & \mathbf{6} & & & \\ \hline
10+2u & 25 & 4+5u & 10 & 5 & u & \mathbf{2} & & \\ \hline
10+2\bar{u} & 4+5\bar{u} & 25 & 10 & \bar{u} & 5 & 0 & \mathbf{2} & \\ \hline
4 & 10 & 10 & 25 & 2 & 2 & 5 & 5 & \mathbf{1}
\end{array}\right). \tag{28}$$

Comparing this matrix with the subdivision matrix (6), we see that it has the same blocks on its diagonal. Thus, if we use the Doo-Sabin weights (17) yet again, the spectrum of the original subdivision matrix becomes

$$\left\{1, \frac{1}{2}, \frac{1}{2}, \underbrace{\frac{1}{4}}_{2n-3\times}, \underbrace{\frac{1}{8}}_{2n\times}, \underbrace{\frac{1}{16}}_{2n\times}, \underbrace{\frac{1}{32}}_{2n\times}, \underbrace{\frac{1}{64}}_{n\times}\right\}. \tag{29}$$

Since all the knots in this scheme are double knots, we need to consider 5×5 vertices in each segment in order to obtain the characteristic map; see Fig. 9.

With $u = e^{-\frac{2\pi \mathbf{i}}{n}\omega}$ as before and defining $h = 2(3086c + 7595)$ we obtain the normalised column vector (again, displayed as a matrix with the element corresponding to $A_0^{1,1}$ lying in the left bottom corner)

$$\begin{aligned}
&\frac{1}{h}\begin{pmatrix}
2170(3c+4) & 31(191c+315) & 5441c+11935 & 30(185c+434) & h \\
2170(2c+3) & 31(127c+245) & 3(1321c+3255) & 2(2196c+5425) & 30(185c+434) \\
1085(3c+5) & 186(16c+35) & 10(333c+868) & 3(1321c+3255) & 5441c+11935 \\
1085(c+3) & 310(5c+14) & 186(16c+35) & 31(127c+245) & 31(191c+315) \\
2170 & 1085(c+3) & 1085(3c+5) & 2170(2c+3) & 2170(3c+4)
\end{pmatrix} \\
&\qquad + \frac{\mathbf{i}s}{h}\begin{pmatrix}
6 & 5 & 3 & 2 & 0 \\
4 & 3 & 1 & 0 & -2 \\
3 & 2 & 0 & -1 & -3 \\
1 & 0 & -2 & -3 & -5 \\
0 & -1 & -3 & -4 & -6
\end{pmatrix}
\end{aligned} \tag{30}$$

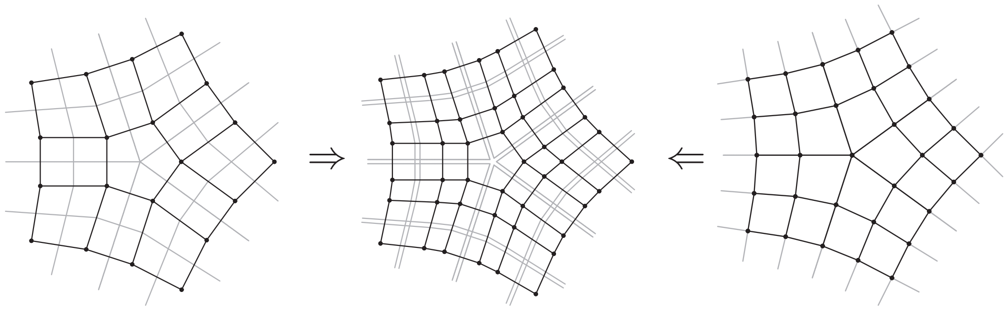

Figure 11: Degree raising and knot insertion: a) to b) via degree raising, c) to b) via doubling every knot.

and its complex conjugate associated with $\lambda_1 = 1/2$ and $\lambda_{n-1} = 1/2$. These give the natural configuration of the scheme; see Fig. 10.

By inspecting the characteristic map of $\mathcal{D}_n$ via the three bicubic patches depicted in Fig. 9 as we did in the case of the $\mathcal{M}_n$ scheme (see Section 2.3), one can show that the map is regular and injective. This proves that the $\mathcal{D}_n$ scheme produces C^1 surfaces for any value of the valency $n \geq 3$.

4. Conclusions and future work

We have investigated binary subdivision schemes derived from cubic B-splines with double knots. Based on results from the univariate case, we presented and analysed two subdivision scenarios: the $\mathcal{M}_n$ scheme using single knot insertion, where n double knots meet at (extraordinary) faces, and the $\mathcal{D}_n$ scheme, where all knots are double and double knot insertion is used. We showed that, with the choice of the original Doo-Sabin weights, both these schemes produce C^1 surfaces. We also pointed out that, whereas the original uniform (bi)cubic scheme is primal, the new schemes exhibit dual behaviour in the vicinity of double knots; see Fig. 11.

These results partially address some of the current limitations of Cashman's NURBS-compatible subdivision framework and open possibilities for further investigation.

Now we present several directions for further research in the areas of subdivision with multiple knots and NURBS-compatible subdivision.

- Higher degrees

  The subdivision matrices of both $\mathcal{M}_n$ and $\mathcal{D}_n$ have the same diagonal blocks as the Doo-Sabin scheme. Thus, for an odd degree $d \geq 5$ scheme with double knots, we conjecture that its subdivision matrix has the same diagonal blocks as the uniform scheme with all knots single at degree $d-1$. This would mean that we could use the same weights as in the uniform schemes of degree $d-1$.

  Starting the same process with degree four B-splines may yield a well behaved C^1 scheme with double (or even triple) knots, this time with Catmull-Clark weights (Catmull and Clark, 1978)p. Also, it is reasonable to expect that higher order schemes of degree d with knots of multiplicity up to $d-1$ will produce C^1 surfaces as well. These considerations are closely related to degree six schemes with quadruple knots generating C^2 surfaces (Reif, 1995; Prautzsch, 1997).

- Dual schemes

  Consider a bivariate, even-degree scheme $\mathcal{S}$ all of whose knots are single, i.e., an even-degree dual scheme. The following steps describe a potential algorithm for including $\mathcal{S}$ among odd-degree schemes by degree raising.

  - Raise the degree of $\mathcal{S}$ by one to obtain a dual odd-degree scheme with extraordinary faces. This comprises doubling all knots and computing new vertices by degree raising; see Fig. 11.

– A subdivision step consists of inserting a double knot into every non-zero knot interval.
– Optionally, after a desired number of iterations remove all double knots by reducing the degree by one.

The open questions here are: how to insert and remove double knots in extraordinary regions (degree raising and reduction) and how to handle such regions themselves in terms of weights.

- Asymmetric configurations

  What about a point where just one double knot comes in along a ray? In such a scenario one can look at the 4-valent case first, as each valency will probably need looking at individually. The Fourier partitioning will not work in this case, but general eigenanalysis should still be applicable, exploiting one reflectional symmetry. Asymmetric configurations also include scenarios where knots with various multiplicities meet.

Acknowledgement. The authors thank EPSRC for supporting this work through grant EP/H030115/1 and the anonymous reviewers for their helpful insights.

References

Ball, A., Storry, D., 1988. Conditions for tangent plane continuity over recursively generated B-spline surfaces. ACM Transactions on Graphics 7 (2), 83–108.

Boehm, W., 1980. Inserting new knots into B-spline curves. Computer-Aided Design 12 (4), 199–201.

Cashman, T. J., Mar. 2010. NURBS-compatible subdivision surfaces. Tech. Rep. UCAM-CL-TR-773, University of Cambridge, Computer Laboratory, (Doctoral thesis).
URL `http://www.cl.cam.ac.uk/techreports/UCAM-CL-TR-773.pdf`

Cashman, T. J., Augsdörfer, U. H., Dodgson, N. A., Sabin, M. A., 2009a. NURBS with extraordinary points: high-degree, non-uniform, rational subdivision schemes. In: ACM SIGGRAPH 2009 papers. ACM, New York, NY, USA, pp. 46:1–46:9.

Cashman, T. J., Dodgson, N. A., Sabin, M. A., 2009b. A symmetric, non-uniform, refine and smooth subdivision algorithm for general degree B-splines. Computer Aided Geometric Design 26 (1), 94–104.

Catmull, E., Clark, J., 1978. Recursively generated B-spline surfaces on arbitrary topological meshes. Computer-Aided Design 10 (6), 350–355.

Chaikin, G. M., 1974. An algorithm for high-speed curve generation. Computer Graphics and Image Processing 3 (4), 346–349.

Cohen, E., Lyche, T., Riesenfeld, R., 1980. Discrete B-splines and subdivision techniques in computer-aided geometric design and computer graphics. Computer Graphics and Image Processing 14 (2), 87–111.

Doo, D., Sabin, M., 1978. Behaviour of recursive division surfaces near extraordinary points. Computer-Aided Design 10 (6), 356–360.

Farin, G., 2002. Curves and surfaces for CAGD: a practical guide, 5th Edition. Morgan Kaufmann Publishers Inc., San Francisco, CA, USA, ISBN: 1-55860-737-4.

Müller, K., Fünfzig, C., Reusche, L., Hansford, D., Farin, G., Hagen, H., Jul. 2010. Dinus: Double insertion, nonuniform, stationary subdivision surfaces. ACM Trans. Graph. 29, 25:1–25:21.

Müller, K., Reusche, L., Fellner, D., April 2006. Extended subdivision surfaces: Building a bridge between NURBS and Catmull-Clark surfaces. ACM Trans. Graph. 25, 268–292.

Peters, J., Reif, U., 1998. Analysis of algorithms generalizing B-spline subdivision. SIAM J. Numer. Anal. 35, 728–748.

Peters, J., Reif, U., 2008. Subdivision Surfaces. Springer Publishing Company, Incorporated, ISBN: 978-3-540-76405-2.

Prautzsch, H., 1997. Freeform splines. Vol. 14. pp. 201–206.

Qin, K., Wang, H., 1999. Eigenanalysis and continuity of non-uniform Doo-Sabin surfaces. In: Proceedings of the 7th Pacific Conference on Computer Graphics and Applications. PG '99. IEEE Computer Society, pp. 179–186.

Reif, U., 1995. TURBS - topologically unrestricted rational B-splines. Constr. Approx 14, 57–78.

Riesenfeld, R., 1975. On Chaikin's algorithm. Computer Graphics and Image Processing 4 (3), 304–310.

Sabin, M., 2010. Analysis and Design of Univariate Subdivision Schemes. Springer, ISBN: 978-3-642-13647-4.

Schaefer, S., Goldman, R., 2009. Non-uniform subdivision for B-splines of arbitrary degree. Computer Aided Geometric Design 26 (1), 75–81.

Sederberg, T. W., Zheng, J., Sewell, D., Sabin, M., 1998. Non-uniform recursive subdivision surfaces. In: Proceedings of the 25th annual conference on Computer graphics and interactive techniques. SIGGRAPH '98. ACM, New York, NY, USA, pp. 387–394.

Warren, J., 1995. Binary subdivision schemes for functions over irregular knot sequences. In: Mathematical Methods in CAGD III. Vanderbilt University Press, pp. 543–562.

Warren, J., Weimer, H., 2001. Subdivision Methods for Geometric Design: A Constructive Approach. Morgan Kaufmann Publishers Inc., San Francisco, CA, USA, ISBN: 1-55860-446-4.